IEEE Access
Multidisciplinary | Rapid Review | Open Access Journal

Date of publication xxxx 00, 0000, date of current version xxxx 00, 0000.

Digital Object Identifier 10.1109/ACCESS.2020.DOI

Modular Design for a Stacked SIW Antenna Array at Ka-band

CLEOFÁS SEGURA-GÓMEZ[1], ÁNGEL PALOMARES-CABALLERO[1], ANTONIO ALEX-AMOR[1,2], JUAN VALENZUELA-VALDÉS[1], PABLO PADILLA[1]

[1]Department of Signal Theory, Telematics and Communications, Universidad de Granada, 18071 Granada, Spain.
[2]Information Processing and Telecommunications Center, Universidad Politécnica de Madrid, 28040 Madrid, Spain.

Corresponding author: Cleofás Segura-Gómez (e-mail: cleofas@ugr.es).

This work was been partially supported by the Spanish Research and Development National Program under Projects TIN2016-75097-P, RTI2018-102002-A-I00, EQC2018-004988-P, the predoctoral grant FPU18/01965, the projects B-TIC-402-UGR18 and P18.RT.4830 of Junta de Andalucía, CEIMar project CEIJ-020 and the University of Granada proyect for young researchers PPJIA2019.10.

ABSTRACT

This paper presents a modular substrate-integrated waveguide (SIW) antenna array based on H-plane aperture structures for Ka-band. The unitary antenna is based on a SIW aperture antenna with an improved H-plane radiation pattern by means of the implementation of metallic vias in the wave propagation along the H-plane antenna. The inner metallic vias are introduced to form four different sub-apertures at the end of the H-plane aperture antenna, dividing the field from the feeding into four in-phase wavefronts. In that manner, a flatter wavefront is generated to achieve high directivity. Additionally, some periodic parallel strips are printed at the end of the antenna aperture to improve the impedance matching with the air. The H-plane antenna is used as the constituting element for an E-plane array antenna, using four H-plane elements. The E-plane array antenna increases the antenna directivity, providing a pencil-shape beam, based on a series coaxial feeding structure. This feeding strategy favours the antenna modularity at the expense of suffering from a slight beam steering with frequency in the working bandwidth. The proposed antenna has an impedance matching below -10 dB from 32.9 to 37.0 GHz (equivalent to 11.73% bandwidth) with a nearly stable gain of almost 10 dBi for the H-plane unitary element and 14 dBi for the E-plane array. Prototypes of both antennas are manufactured to validate the proposed unitary antenna and array designs.

INDEX TERMS Antenna array, millimeter-wave, modular design, SIW antenna

I. INTRODUCTION

NOWADAYS, the increase on the operating frequency of the devices is a necessity due to the current saturation of the bands below 6 GHz [1], [2]. However, one of the main limitations when the frequency increases is the higher resulting propagation loss for a given distance [3]. This limitation forces the use of highly directional antennas with narrow beam width. Among the technologies available to design these radiating devices, planar technologies such as microstrip [4] or substrate integrated waveguide (SIW) [5] are drawing attention because of their low-cost and easy implementation in a complete system [6]–[8]. Especially, SIW technology provides better performance in terms of losses when the frequency increases compared to microstrip technology [9]. Moreover, SIW technology keeps the designs compact and simple even at high frequencies such as millimeter-wave bands [10]. Nevertheless, the dielectric losses at the upper bands of the millimeter-wave range should be taken into consideration because they may be not negligible.

Different strategies in the design of high directive antennas implemented in SIW are proposed in the literature. One of the approaches to enhance the directivity of an antenna system is to form an array. SIW antenna arrays at high frequencies employ a corporate feeding network to equally distribute the input power among the antennas [11]–[15]. The corporate feeding network is implemented in SIW to reduce the propagation losses while the radiating elements can be implemented in other technologies as it is observed in [11] or [12]. Leaky-wave antennas is another design to achieve a high directive SIW antenna [17]–[19]. Nevertheless, the nature of the leaky-wave antennas makes the beam steers with the frequency. This fact makes this type of antennas unsuitable in general for point-to-point communications but

This article has been accepted for publication in a future issue of this journal, but has not been fully edited. Content may change prior to final publication. Citation information: DOI 10.1109/ACCESS.2020.3020471, IEEE Access

they can find applications in radar systems. In [20], it is proposed a solution to avoid the beam squinting in a SIW leaky-wave antenna by using a corrective prism next to the antenna aperture. Alternatively, in [21] is demonstrated that an air-filled SIW leaky-wave antenna reduces the beam deviation at certain frequency range. The use of lenses is an another solution to realize a planar phase front in order to feed an array in phase and with different ports. Different types of lenses such as Rotman [22], Cassegrain [23], Luneburg [24] or parabolic reflector [25] have been used in SIW 2D arrays for multibeam applications.

The end-fire SIW antenna is an attractive solution to design antennas with high-directivity, low-profile and easy integration [26]. The main drawback of this type of antennas is the existing phase error at the antenna aperture [27]. Several approaches to resolve this problem have been proposed. In [28], metallic vias are introduced along the horn to correct the phase front at the aperture increasing the directivity in comparison with a traditional SIW horn antenna. A similar approach to correct the phase front is used in [29] but, the apertures are loaded with antipodal linearly tapered slot antennas and they are stacked in order to carry out a monopulse antenna. Alternatively, the work in [30] achieves the correction of the phase front by using longitudinal gaps in the upper and lower copper layers and along the H-plane horn antenna. Additionally, a transition between the substrate and the air at the antenna aperture is implemented in order to increase the gain of the antenna. In [31], it is proposed an air-filled SIW horn with corrected phase front by using hard side walls and profiling them. The use of a dielectric with circular or elliptical shape in front of the horn aperture is also demonstrated to narrow the beam width in both planes and thus, enhancing the directivity [32]. Recently, a pyramidal horn antenna is proposed in [33] by stacking different SIW layers forming a feeding network to distribute the power among H-plane horn SIW antennas. However, the design provides narrow bandwidth because of the complex feeding network design. Finally, the work in [34] presents a vertical stack of two SIW horn antenna in order to increase the directivity in the E-plane.

This paper presents a modular design for a stacked SIW antenna array at Ka-band. The unitary antenna is based on a SIW horn antenna with an improved H-plane radiation pattern by means of the implementation of metallic vias in the wave propagation along the horn antenna. Since this antenna lacks of a narrow E-plane, an array in the vertical plane is formed by stacking a number of unitary antennas fed by a coaxial line in order to increase the directivity. The main contribution of this work is to provide a cost-effective modular design, whose radiation properties can be varied depending on the number of H-plane antenna elements considered for the final array. With this modular design there is no necessity of antenna redesign, since no modification in the unitary antenna is made to form the E-plane antenna stack. However, the series nature of the array feeding network introduces a progressive beam steering with frequency,

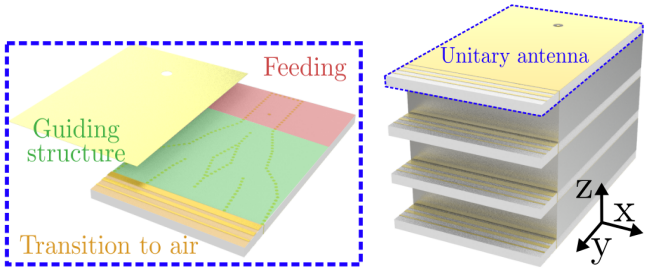

(a) (b)

FIGURE 1: Antenna designs: (a) H-plane unitary antenna, and (b) E-plane array antenna.

similar to the one of leaky wave antennas. This fact, joined to the inherent increase of losses and the difficulty in controlling the uniformity of the power distribution, makes advisable not to use a large number of H-plane antenna elements for the array. In this work, four elements are selected as an adequate trade-off choice for the antenna performance regarding these limitations. The document is organized as follows. Section II presents the design of the H-plane unitary antenna. Section III depicts the E-plane array design based on the H-plane unitary antenna. Section IV provides the experimental validation of the design through prototypes and their the measurements. Finally, the conclusions are drawn in Section V.

II. H-PLANE UNITARY ANTENNA DESIGN

The proposed H-plane unitary antenna and the complete E-plane array are illustrated in Figs. 1(a) and 1(b), respectively. The unitary antenna has three main parts: the feeding interface, the guiding structure and the transition to the air. The feeding part is based on coaxial to waveguide transition that is described in the following subsection. The next part is the guiding structure that enhances the phase front at the aperture of the horn antenna in order to increase the directivity. The last part, the transition to the air, is implemented to reduce the impedance mismatching between the antenna aperture and the air. The E-plane array is formed by stacking a number of H-plane unitary antennas in the z direction. In this manner, the directivity in the E-plane (YZ plane) is enhanced since the H-plane horn antennas only provide a high directivity level in the H-plane (XY plane).

Since the employed technology is SIW, the configuration of the metallized vias has to be properly selected in order to avoid field leakage in the wave propagation. Fig. 2 shows an inside view of the unitary antenna (without the transition to air) highlighting the metallized vias that compose the design. The distance between vias d and the radius of the vias r are selected to be 0.8 mm and 0.25 mm, respectively. These dimensions along with a relative dielectric constant ϵ_r of 3.55 ensure the good performance of the SIW in the operating frequency band based on the following conditions [35]:

$$d \leq 4r \tag{1}$$

This article has been accepted for publication in a future issue of this journal, but has not been fully edited. Content may change prior to final publication. Citation information: DOI 10.1109/ACCESS.2020.3020471, IEEE Access

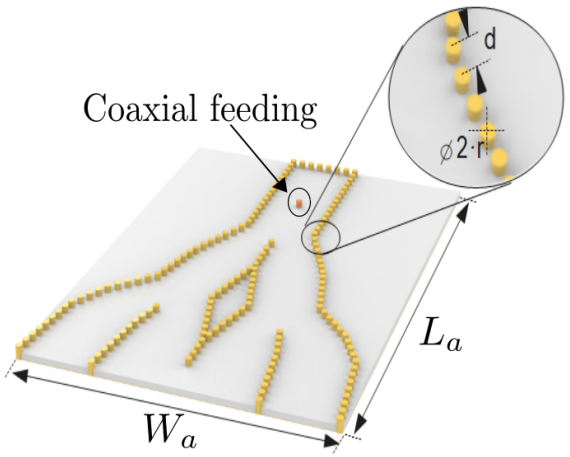

FIGURE 2: Geometrical configuration of the proposed H-plane unitary SIW antenna. Dimensions are: L_a = 38.9 mm and W_a = 23.9 mm.

$$2r < \lambda_g/5 \tag{2}$$

where λ_g is the guided wavelength in the SIW. In addition, the coaxial feeding, which is at the opposite side of the antenna aperture, is also illustrated. The top and bottom copper plates of the SIW have a thickness of 35 μm.

A. FEEDING STRUCTURE DESIGN

Considering that the antenna works in the Ka-band, a coaxial connector is a simple and feasible option to achieve a cost-effective and compact feeding. Since the antenna is implemented in SIW technology, a proper transition from coaxial to SIW is required. This transition has to convert the fundamental mode of the coaxial line (TEM mode) to the fundamental mode of the waveguide that is the TE_{10} mode. Tapered transitions are an interesting solution to increase the operating bandwidth in the mode conversion [36], [37], especially in all-metal aperture antennas where the shape of the antenna can be easily adjusted with milling techniques. However, the manufacturing complexity typically prevents its usage in SIW technology. A simpler solution is the implementation of a quarter-wavelength short-circuited waveguide section, at the expense of a reduction of the frequency bandwidth. Some views of the designed transition are shown in Figs. 3(a) and 3(b). In order to avoid mismatching between the coaxial line and the waveguide, a waveguide short is located at the back of the transition to provide a in-phase reflection. The wave towards the back wall has a delay of $\lambda_g/4$ and $\lambda_g/4$ in return. This fact together with the 180º phase shift introduced by the reflection at the back wall forces an in-phase summation of the reflected wave with the excited one from the coaxial probe. The distance L is adjusted to be quarter of the wavelength at 35 GHz with an extra wavelength to prevent difficulties in the manufacturing of a short distance between the coaxial probe and the back wall. Figs. 3(c) and

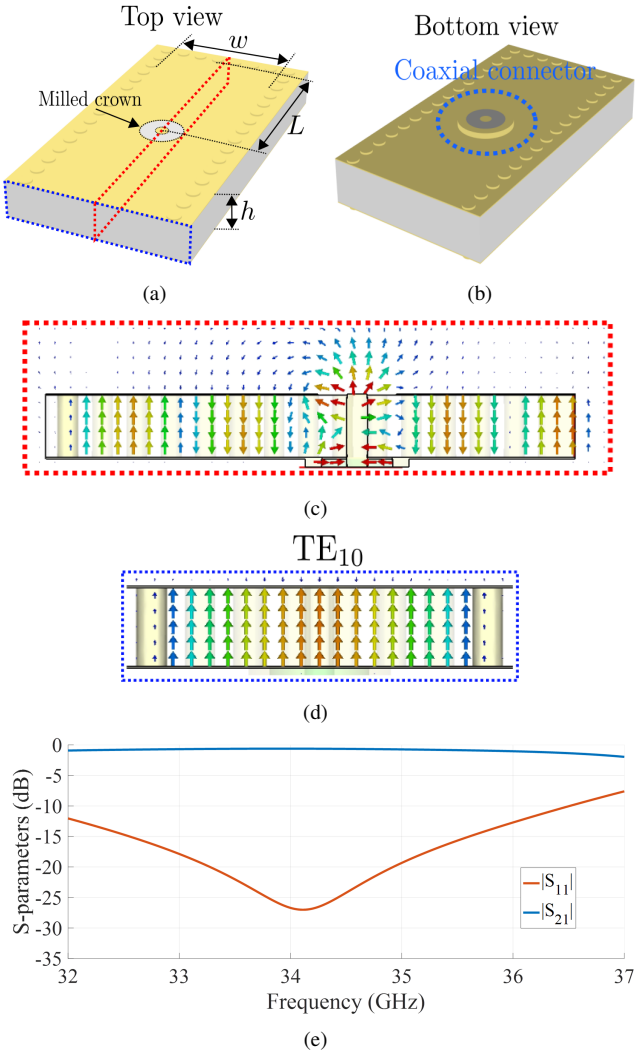

FIGURE 3: Coaxial to SIW transition: (a) top and, (b) bottom views of the design. Dimensions are: w = 5.1 mm, L = 6.45 mm and h = 1.52 mm. (c) Transversal and longitudinal cut views showing the electric field distribution, and (d) Simulated transmission and reflection coefficients.

3(d) illustrate the electric field distribution in the transition for different cut views. The coaxial probe length reaches the upper copper plate of the SIW. At this point, a milled crown is inserted to provide impedance matching for the transition. For antenna stacking, the coaxial feed line must completely pass through the substrate of the coaxial to SIW transition. The milled crown avoids the short-circuit of the coaxial with the upper copper layer of the SIW improving the performance of the transition. In the output port of the transition (framed in blue), the TE_{10} mode is obtained as it is observed in Fig. 3(d). The transmission and the reflection coefficients of the coaxial to SIW transition are illustrated in Fig. 3(e). From 32 GHz to 36.5 GHz, it is achieved an impedance matching bandwidth below -10 dB with a good level of transmission to the SIW.

The milled crown is an important element to enable the modularity of our antenna design since it allows a coaxial

This article has been accepted for publication in a future issue of this journal, but has not been fully edited. Content may change prior to final publication. Citation information: DOI 10.1109/ACCESS.2020.3020471, IEEE Access

feeding distribution in the vertical stack of unitary antennas, as it will show in the next section. However, this element can provoke reduced radiation losses because the SIW is not completely shielded. In Fig. 3(c), it is illustrated the longitudinal cut view of the transition showing the electric field distribution. At the end of the coaxial probe, it is observed that a reduced amount of electric field is radiated due to the milled crown. A study of the radiation losses provided by the existence of this element is shown in Fig. 4. This Fig. presents the percentage of the input power that is undesirably radiated throughout the milled crown. Although there exists losses, they are low and acceptable to permit the design of the stacked antenna array.

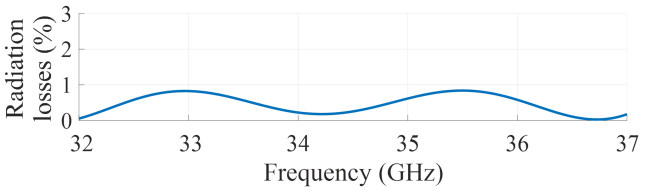

FIGURE 4: Radiation losses in the coaxial to SIW transition.

B. GUIDING STRUCTURE DESIGN

Once the SIW transition has been depicted, the guiding structure is presented in this subsection. The aim of the guiding structure is to provide a flat phase front at the end of the H-plane horn antenna where the radiation is produced. In order to achieve this target, consecutive waveguide divisions are implemented in the aperture antenna, as it can be observed in previous Fig. 2. This guiding structure begins at the end of the coaxial to SIW transition and ends at the edge of the antenna aperture. The propagation of the wave along the aperture is modified both in amplitude and phase to obtain nearly constant phase and equally distributed power at the radiating part. For this purpose, the width of the waveguide divisions along the aperture has been adjusted to control the propagation constant (β_g) and reduce the phase difference at the end of the antenna aperture maintaining an uniform amplitude at this point. The result is illustrated in Fig. 5 where the electric field inside the aperture is shown for different frequencies. The figure reveals that at the end of the aperture the wave arrives with low phase difference and with an approximately uniform amplitude along the end of the antenna aperture (x direction).

C. SUBSTRATE TO AIR TRANSITION AND COMPLETE DESIGN

For end-fire antennas based on SIW, there exists an impedance mismatching between the air and the waveguide filled with dielectric. Therefore, an impedance matching element is needed to improve the radiation of the antenna. By means of the addition of some parallel strips on the top and bottom copper layers of the SIW structure, the antenna can be properly matched with the air [38]. The employed transition is illustrated in Fig. 6. The impedance matching

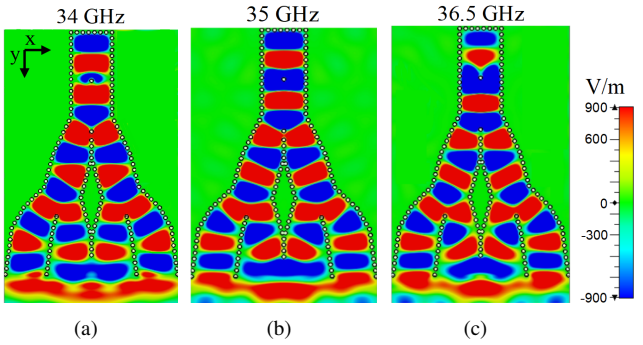

FIGURE 5: Electric field distribution inside the aperture of the antenna at: (a) 34 GHz, (b) 35.25 GHz and, (c) 36.50 GHz.

bandwidth of the antenna is provided by combining horizontal metallic and air strips, progressively reducing the width of the metallic strips (l_c) and enlarging the air strip width (l_a). Each pair of metallic plus air strips have a width of about quarter of the guided wavelength at the center frequency. Specifically for this transition, the percentage of metallic strip is 80%, 50% and 20% for the first, second and third pair of strips, respectively. The air strip is the complementary for its corresponding metallic strip. In Fig. 7(a), it is shown the reflection coefficient of the unitary antenna with and without the substrate to air transition. The impedance bandwidth is clearly improved with implementation of the depicted transition. Moreover, it is demonstrated that only a few pair of strips are required to get a proper impedance matching with the air interface.

Regarding the radiation performance, Fig. 7(a) represents the directivity that the antenna provides in the frequency band. The target operation bandwidth ranges from 34 GHz to 36.5 GHz since the guiding structure has been designed at a center frequency of 35.25 GHz. The directivity is around 10 dBi in this frequency range. A drop in the directivity is observed at 34.5 GHz. This small decrease in the directivity appears due to the increase of the side lobe levels at this frequency. The side lobe levels are directly related to the flatness of the wavefront phase in the aperture. Figs. 7(b), 7(c) and 7(d) illustrate the 3-D far-field radiation pattern of the antenna at different frequencies. The H-plane configuration of the unitary antenna present a fan-beam pattern that concentrates the radiation in the H-plane, while the E-plane remains with a broad beamwidth. An array in the vertical direction is needed to improve the directivity and convert the current radiation pattern into a pencil-beam pattern.

III. E-PLANE ARRAY ANTENNA DESIGN

This section is devoted to the design of the E-plane array using the H-plane antenna as constituting unitary antenna of the four elements array (Fig. 8(a)). Since a narrow beamwidth shape in the H-plane has been achieved with unitary antenna, beamwidth shaping in the E-plane is now required. This is carried out by means of vertically stacking a set of unitary antennas. In order to feed the vertical stack of unitary antennas,

This article has been accepted for publication in a future issue of this journal, but has not been fully edited. Content may change prior to final publication. Citation information: DOI 10.1109/ACCESS.2020.3020471, IEEE Access

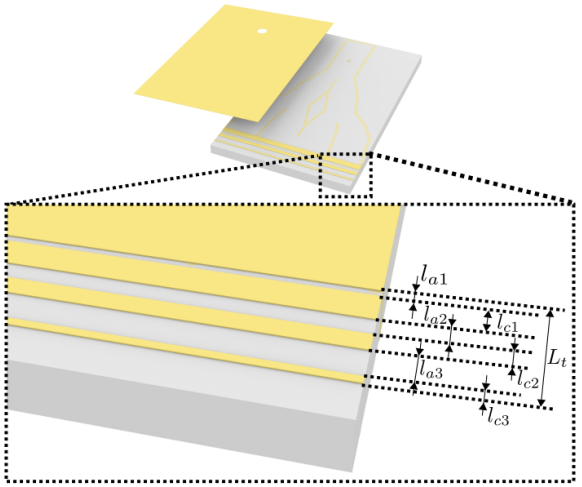

FIGURE 6: Transition from SIW to air. Dimensions are: l_{a1} = 0.27 mm, l_{a2} = 0.67 mm, l_{a3} = 1.06 mm, l_{c1} = 1.06 mm, l_{c2} = 0.67 mm, l_{c3} = 0.27 mm and, L_t = 4 mm.

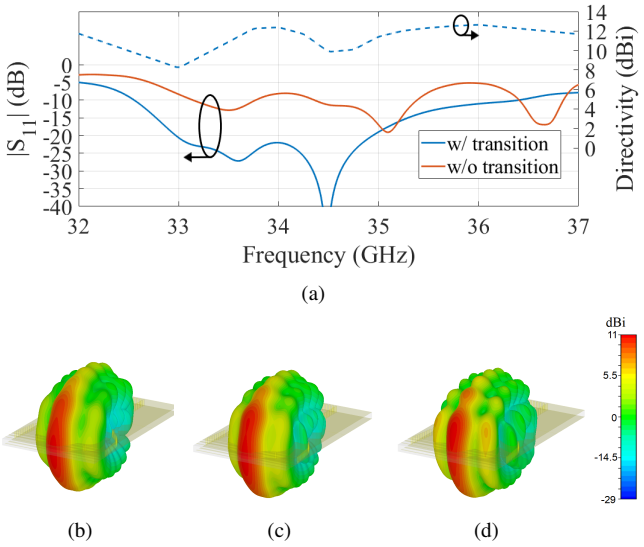

FIGURE 7: Performance of the H-plane unitary antenna: (a) $|S_{11}|$ and directivity. Radiation patterns at: (b) 34 GHz, (c) 35.25 GHz and, (d) 36.50 GHz.

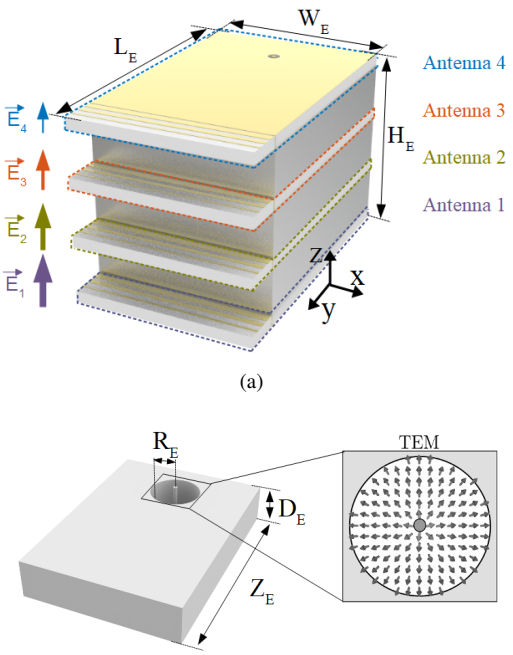

FIGURE 8: Array design: (a) configuration of unitary stacked antennas. Dimensions are: W_E = 23.90 mm, L_E = 38.88 mm and H_E = 24.34 mm. (b) Metallic spacing block to separate the unit antennas. Dimensions are: Z_E = 33.5 mm, D_E = 6.00 mm and R_E = 4.00 mm.

a series coaxial feeding is implemented. The coaxial feeding requires to extend the coaxial conductor through the milled crowns of the antenna that form the array. In this manner, the input power is distributed into all the H-plane antennas.

A. PROGRESSIVE COAXIAL FEEDING

The E-plane array feeding implies a coaxial feeding that progressively feeds the four antennas in series. Considering the necessary electric distance between H-plane antennas in the array to avoid grating lobes, it is necessary to add some spacing metallic blocks between the antennas, preserving the coaxial configuration to properly transmit the coaxial mode that feeds each antenna along the array of stacked unitary antennas. An important aspect that has to be accounted is the phase shift introduced by the coaxial series feeding at each antenna port. A certain level of impedance mismatch between the antennas is inevitable but can be mitigated by improving the diameter of the metallic spacing blocks. The radius and the thickness of these metallic spacers are adjusted to achieve the best array factor without impairing the reflection coefficient. The thickness of the metallic spacers determines the inter-antenna phase values. The best trade-off among grating lobes, tilt angles range and directivity is achieved for a distance between antenna elements of $0.86\lambda_o$, being λ_o the vacuum wavelength at the center frequency of the array design. The metallic spacer model is shown in Fig. 8(b), the parameter D_E is the height of the plates, set to 6 mm, so that the final inter-antenna distance is approximately 7.5 mm. This distance does not cancel out the inter-antenna phase difference that will imply a vertical beam tilt, but optimizes the structure matching. The radius of the plate, R_E, is set to 4 mm to form a transmission line for the coaxial feeding (coaxial mode) and to encourage the series feeding. The length Z_E is not of importance in the array configuration and is set to the same value as the length of the antenna without the transition.

Figs. 9(a) and 9(b) display the S-parameters in amplitude and phase of the coaxial feeding structure without taking into account the antenna elements. Fig. 9(a) shows the level of transmission that reaches at each antenna port. There is a decrease in the receiving as the antenna is further from the input port. The phase difference along the frequency range

This article has been accepted for publication in a future issue of this journal, but has not been fully edited. Content may change prior to final publication. Citation information: DOI 10.1109/ACCESS.2020.3020471, IEEE Access

between antennas is shown in Fig. 9(b). The progressive feeding makes the phase differences between antennas frequency dependent. These amplitude and phase values have been previously adjusted and employed to achieve an array factor [39] that minimizes the main lobe tilt in the E-plane, which exists inherently by the progressive feeding. Moreover, in this manner, the whole simulation of the antenna array is saved and only the feeding structure of the array is computed. This provides a good approach of the final radiation performance in the E-plane. As the total progressive phase shift between the lower and upper antenna is less than 180º, there is no zero between them and this results in a main lobe tilt in the E-plane, which can be easily mechanically corrected. Fig. 9(c) presents the simulated directivity (the whole antenna array is computed) when additional antennas are added to the array taking into account the progressive phase shift and the designed inter-distance between antennas. It is observed an increase in the directivity when additional antennas are stacked. A noticeable increase of the directivity is observed when the unitary elements are stacked. However, the amplitude decay associated to the series feeding (Fig. 9(a)) provokes that the stack of several unitary antennas has no longer influence on the increase of the directivity.

With the increase in the number of H-plane antennas in the array, the unwanted effect of main lobe deflection also occurs. When four antennas are stacked for the array design, deviations of no more than 9º are produced along the working frequency band.

B. ARRAY DESIGN

The final dimensions of the E-plane array when the unitary antennas are stacked are 38.9 mm x 23.9 mm x 24.4 mm. Both the unitary element and the antenna array are linearly polarized, with the electric field oriented along the z direction according the propagating TE_{10} mode in the SIW. Fig. 10(a) displays the electric field (E-field) distribution at the central frequency of the working band. Figs. 10(c)-(e) show the 3-D far-field radiation patterns. A slight tilt in the main lobe is observed. This fact is due to two reasons, the small phase differences between antennas and the reflections occur at the metallic spacing block when the antennas radiate. In Fig. 10(b), the $|S_{11}|$ parameter of the final array design is shown. As it can be observed, the bandwidth is reduced for the array design due to the limitations of the series feeding.

IV. PROTOTYPES AND MEASUREMENTS

Once the design is finished, the prototype is manufactured and measured. The realized manufactured relative permittivity (ϵ_r) of the substrate is 3.55, in accordance with the dielectric constant considered for the design. The manufacturing cost is reduced with respect to other fabrication techniques, being able to manufacture several units for a reduced cost difference compared to one unit due to circuit board mass-production. The connector used is a 2.4 mm SMA coaxial connector with 50 Ω impedance. The process of set-up (alignment and measurement of pattern) is observed

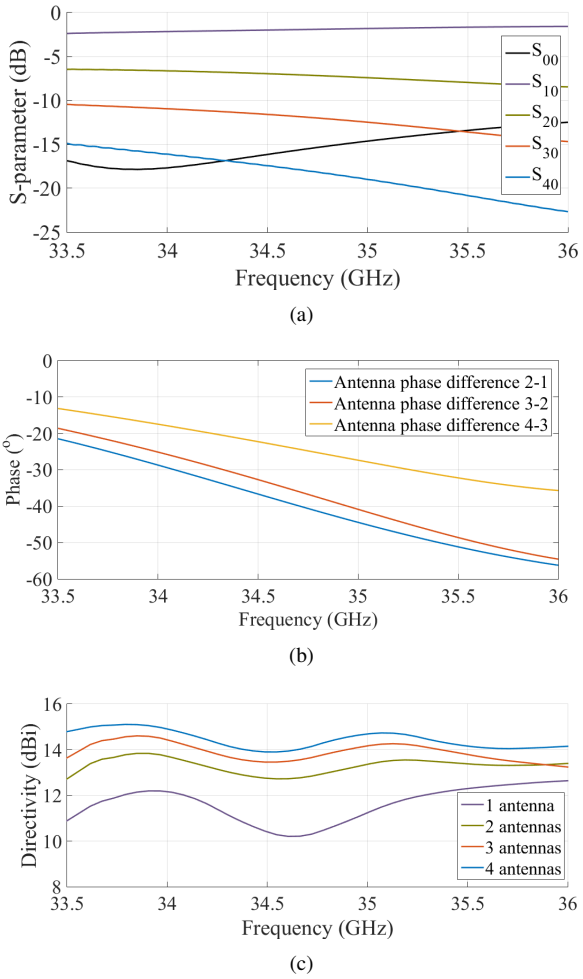

FIGURE 9: Feeding of the array: (a) S-parameters referred to the feeding coaxial port (port 0) without antennas, (b) Phase difference between antennas without antennas, and (c) directivity increase for each additional antenna added to the array.

in Fig. 11(a) and 11(b). This assembling process and the measurements have been carried out at the millimeter-wave antenna measuring facilities of the University of Granada.

A. UNITARY ANTENNA CHARACTERIZATION

Figs. 12(a) and 12(b) show the prototype of unitary antenna along with the 2.4 mm connector to feed the antenna. In the measurement process, a transition from 1.85mm to 2.92mm (compatible with 2.4mm connector) was used and the cable of the vector network analyzer (VNA) R&S-ZVA67 was calibrated up to the 1.85mm connector. The measured reflection coefficient is illustrated and compared to the simulated one in Fig. 12(c). The measured matching band is in accordance with the design simulation one and only a slight deviation is observed. This slight frequency shift (1%) may be due to tolerances in the value of the manufactured permittivity, positions of the vias or length of the coaxial feeding.

The realized band in terms of matching is larger than the simulated band, so the final working matching band is

This article has been accepted for publication in a future issue of this journal, but has not been fully edited. Content may change prior to final publication. Citation information: DOI 10.1109/ACCESS.2020.3020471, IEEE Access

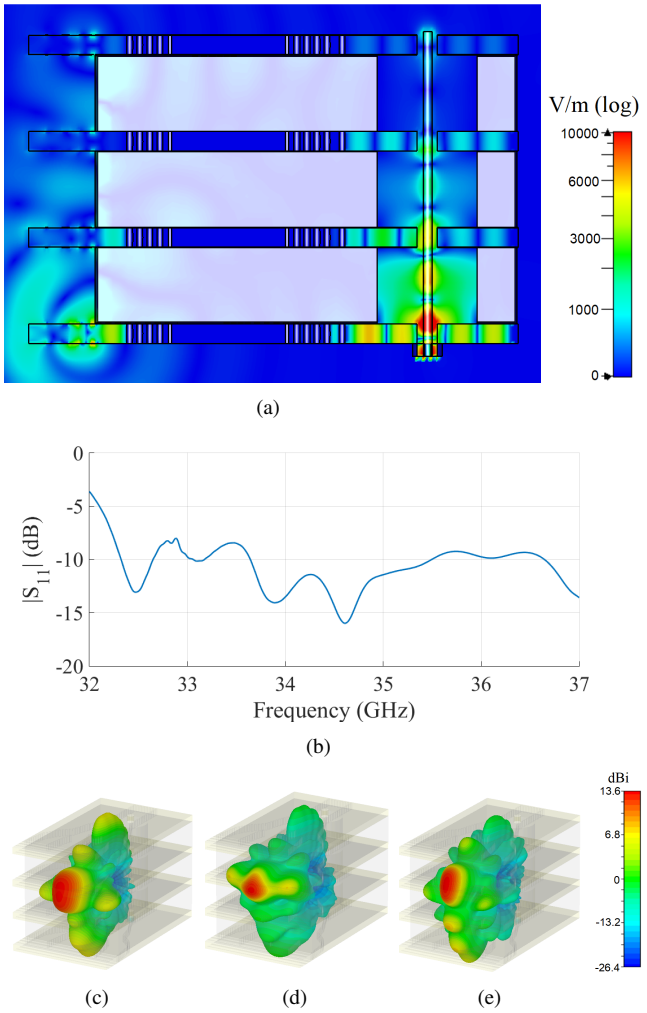

FIGURE 10: Array E-plane: (a) electric field distribution in absolute value at 35.00 GHz of the coaxial mode, (b) $|S_{11}|$ of the array. Radiation patterns at: (c) at 34 GHz, (d) 35 GHz and, (e) 35.75 GHz.

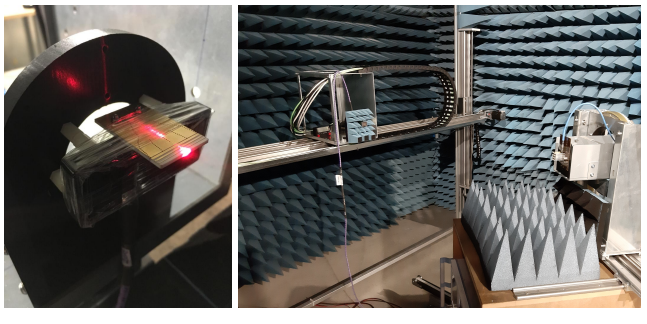

FIGURE 11: Antenna measurements set-up: (a) antenna alignment process, and (b) pattern measuring set-up.

defined from 32.9 GHz to 37.0 GHz. The center frequency is 34.95 GHz achieving 11.73% of relative bandwidth. However, as it will be described below, the frequency band is limited by the antenna gain due to the frequency range for a

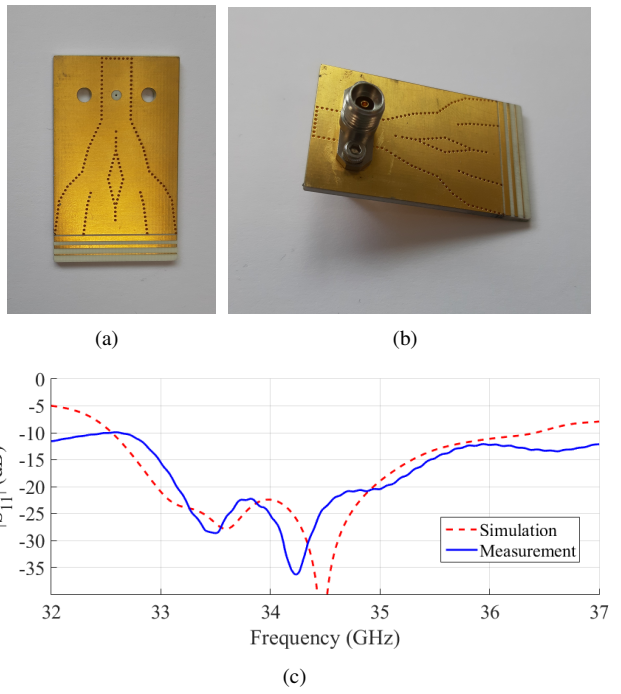

FIGURE 12: Antenna prototype: (a) upper view, (b) bottom view, and (c) $|S_{11}|$.

proper directive pattern configuration of the antenna design.

The H-plane (XY plane) radiation patterns at different frequencies are shown in Figs. 13(a), 13(c) and 13(e). Directive radiation patterns are observed in the operating frequency band of the manufactured antenna. In higher frequencies, the main lobe is narrower and the directivity tends to increase. There is also a proper correspondence between the shapes of the simulated and measured radiation patterns. For the sake of completeness, it has been measured 2-D far-field radiation patterns that are displayed in Figs. 13(b), 13(d) and 13(f). A high directivity is observed at the H-plane. In constrast, the E-plane (YZ plane) does not provide a directive beam, as expected in the design process.

Additionally, the gain of the antenna is measured and it is illustrated in Fig. 14. A stable gain of about 10 dBi is achieved from 33.75 GHz at 34.5 GHz and from 35.25 GHz at 36.5 GHz. In addition, the mean efficiency value is 64.30% from 32.75 to 37 GHz.

B. ARRAY ANTENNA CHARACTERIZATION

Once the unitary antenna has been measured and conveniently characterized, the complete array antenna has been assembled and measured for its validation. The final prototype is displayed in Fig. 15(a) and 15(b). Fig. 15(c) provides the matching outcomes of the array prototype. As it can be stated, the $|S_{11}|$ value in frequency varies slightly compared to the one of the unitary antenna. This is due to the progressive feed which is the most limiting element of the array and suffers from manufacturing and assembling tolerances. The difference between the simulated and measured matching

This article has been accepted for publication in a future issue of this journal, but has not been fully edited. Content may change prior to final publication. Citation information: DOI 10.1109/ACCESS.2020.3020471, IEEE Access

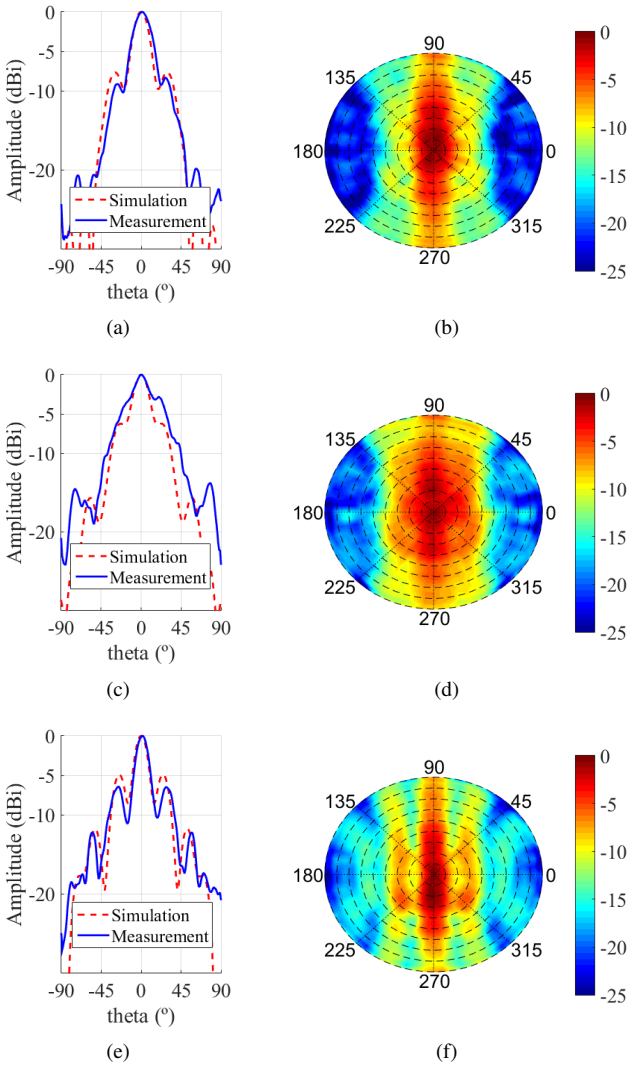

FIGURE 13: Unitary antenna measurements: (a) 34.00 GHz H-plane radiation pattern, (b) Radiation pattern (2-D far-field) at 34.00 GHz, (c) 35.25 GHz H-plane radiation pattern, (d) Radiation pattern (2-D far-field) at 35.25 GHz, (e) 36.50 GHz H-plane radiation pattern, and (f) Radiation pattern (2-D far-field) at 36.50 GHz.

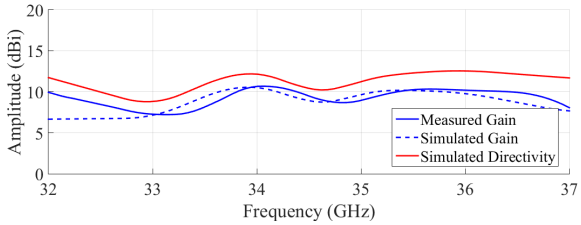

FIGURE 14: Gain of unitary antenna (simulated and measured values) and simulated directivity.

levels may be due to: i) the losses in the SMA connector and its particularities when added to the E-plane array prototype and ii) any additional increase in the losses of the substrate material that would result in an improvement of the prototype matching at the expense of having a higher level

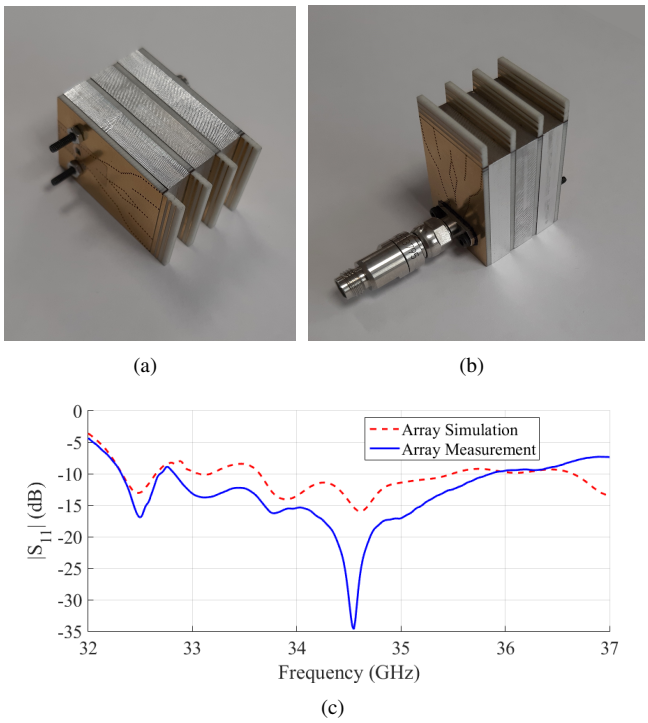

FIGURE 15: Array prototype: (a) perspective view (upper), (b) perspective view (bottom), and (c) $|S_{11}|$.

of inner losses. In any case, comparing the simulations to the measured results, it is stated that the measured matching of the antenna is adequate in the desired bandwidth and its gain value is in the expected range in the band of interest for the design. The final working band is defined from 33.8 GHz to 35.8 GHz. The center frequency is 34.8 GHz and in this case the relative bandwidth is reduced to 5.74% with respect to the unitary antenna due to the frequency limitations of the serial feed of the array.

Regarding the radiation performance of the array antenna, the 2-D far-field spherical radiation pattern of the antenna has been measured at the central frequency a at the lower and upper frequency limits, depicted in Figs. 16(b), 16(d) and 16(f). Additional details of the 2D cuts for the E-plane are shown in Figs. 16(a), 16(c) and 16(e). It can be observed that the simulated radiation patterns and the measured ones have a good agreement, especially in the main lobes. Small differences between the simulated and the measured tilt angles are found, particularly when the frequency increases. This may be due to tolerances in the input phases provided by the manufactured progressive feeding.

Another remarkable feature of the array antenna is the high gain value achieved. In Fig. 17 the measured gain of array is illustrated along with the expected simulated value. One critical issue is the gain fluctuations in the desired frequency band, that are mainly due to the progressive feed in the array structure. Compared to the unitary antenna, the gain value is stable and has a similar shape than the one of the unitary antenna gain, but about 4 dBi higher, as the array

This article has been accepted for publication in a future issue of this journal, but has not been fully edited. Content may change prior to final publication. Citation information: DOI 10.1109/ACCESS.2020.3020471, IEEE Access

TABLE 1: Comparison between proposed and referred SIW antenna arrays at Ka-band

Ref.	Frequency Band (GHz)	Polarization	Max. Gain (dBi)	Beam Deviation (º)	Scale	Feeding	Modular
[12]	35.3-35.55	Circular	18.14	0	4x4	Corporate Feed Network	No
[15]	32-43	Circular	12.8	±38	1x4	Butler Matrix	No
[19]	34-36	Linear	12.5	41	1x6	Six-way Cavity	No
[33]	35.1	Linear	13.1	0	1x4	Four-way Splitter	No
This work	33.8-35.8	Linear	14.14	9	1x4	Series Coaxial	Yes

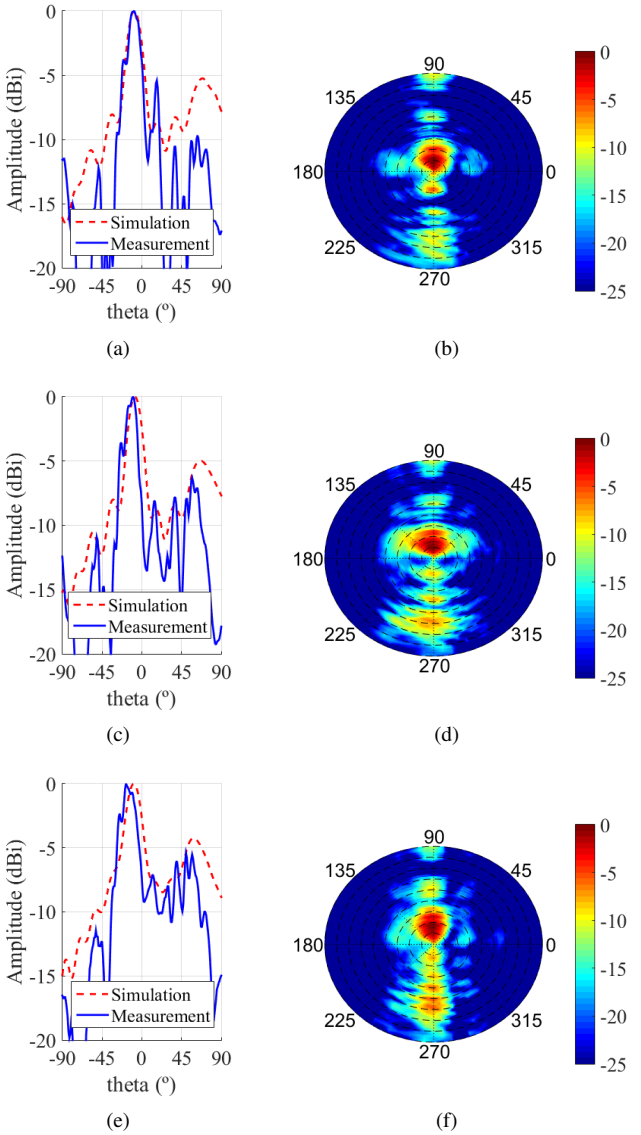

FIGURE 16: Array antenna measurements: (a) 34.00 GHz H-plane radiation pattern, (b) Radiation pattern (2-D far-field) at 34.00 GHz, (c) 35.00 GHz H-plane radiation pattern, (d) Radiation pattern (2-D far-field) at 35.00 GHz, (e) 35.75 GHz H-plane radiation pattern, and (f) Radiation pattern (2-D far-field) at 35.75 GHz.

configuration forces the E-plane pattern main lobe to be sharper and thinner. In addition, the mean efficiency value of the array is 67.88% in the working band.

Finally, the Table 1 presents a comparison among the reported SIW antenna arrays and the proposed one. Different types of arrays designs have been included for a complete comparison. For instance, the work in [15] presents an endfire array based on a Butler matrix with multibeam capability whose scanning range is indicated in the table. Conversely, the work in [33] provides an antenna design with no scanning capability. The proposed antenna array presents a frequency band and maximum gain comparable to other works with the advantage of its modularity. This unique characteristic is achieved at the expense of a beam deviation along the frequency of 9º due to the progressive coaxial feeding. In [19], the authors present an hexagonal array based on rapid beam-scanning leaky wave antennas to provide omnidirectional radiation. Compared to the proposed antenna array, our design accomplishes a cost-effective way to arrange H-plane aperture antennas to shape the main beam in the E-plane as it shown in the 2-D radiation patterns of Fig. 16. This fact provides a modular capability that is not observed in other SIW antenna arrays.

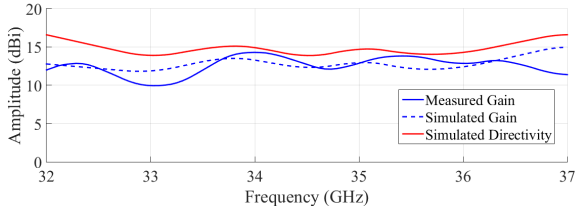

FIGURE 17: Gain of array antenna (simulated and measured values) and simulated directivity.

V. CONCLUSION

This paper presents a modular SIW antenna design based on a stacked composition of H-plane aperture antenna structures, conceived as a proof-of-concept for SIW antenna design in the Ka-band. The H-plane aperture antenna structure is designed through aperture splits by means of metallic via holes, conforming four joined waveguides ended with apertures. The design economizes the number of vias needed in the separation rows and focuses the field at the aperture to enhance the directivity of the antenna. The main contribution of this work is the cost-effective modular design, whose radiation properties can be varied depending on the number of unitary H-plane antenna elements considered for the final E-plane array. The series coaxial feeding strategy for the array favours the antenna modularity at the expense of suffering from a slight beam steering with frequency in the working

bandwidth. This modular design avoids the necessity of redesign when varying the number of antenna elements, since no modification in the unitary antenna is made to form the E-plane antenna stack.

According to the laboratory measurements, there is a proper agreement between the simulations and the the prototype outcomes. The radiation pattern performance of the proposed antenna is very directive due to the equalized phase front formed by the flat wavefronts on the four waveguide apertures that compose the antenna radiating interface. An average stable gain in the operating frequency band of almost 10 dBi has been achieved. This band is between 32.9 GHz and 37.0 GHz. Once its performance has been validated, the H-plane aperture antenna structure is used as the unitary antenna to create an array of four stacked elements. As a consequence, the directivity is increased due to the E-plane pattern distribution, which becomes highly directional. This proof-of-concept of SIW array antenna design at Ka-band demonstrates the feasibility of future modular designs for 5G systems with this technology and takes advantage of board circuit mass production to assemble cost-effective SIW arrays.

REFERENCES

[1] T. S. Rappaport, S. Sun, R. Mayzus,. H. Zhao, Y. Azar, K. Wang. "Millimeter Wave Mobile Communications for 5G Cellular: It Will Work!", *IEEE Access*, vol. 1, pp. 335 - 349, May 2013.

[2] J. Zhang, X. Ge, Q. Li, M. Guizani and Y. Zhang, "5G Millimeter-Wave Antenna Array: Design and Challenges," *IEEE Wirel. Commun.*, vol. 24, no. 2, pp. 106-112, April 2017.

[3] L. Wei, R. Q. Hu, Y. Qian and G. Wu, "Key elements to enable millimeter wave communications for 5G wireless systems'", *IEEE Wirel. Commun.*, vol. 21, no. 6, pp. 136-143, December 2014.

[4] D. M. Pozar and D. H. Schaubert. *Microstrip Antennas: The Analysis and Design of Microstrip Antennas and Arrays*, Wiley, 1995.

[5] D. Deslandes and K. Wu, "Integrated microstrip and rectangular waveguide in planar form", *IEEE Microw. Wireless Compon. Lett.*, vol. 11, no 2, pp. 68-70, Feb. 2001.

[6] P. H. Rao, S. Sujitha and K. T. Selvan, "A Multiband, Mutipolarization Shared-Aperture Antenna: Design and evaluation," *IEEE Antennas Propag.* Mag., vol. 59, no. 4, pp. 26-37, Aug. 2017.

[7] N. Ojaroudiparchin, M. Shen, S. Zhang and G. F. Pedersen, "A Switchable 3-D-Coverage-Phased Array Antenna Package for 5G Mobile Terminals," *IEEE Antennas Wireless Propag. Lett.*, vol. 15, pp. 1747-1750, 2016.

[8] C. Di Paola, K. Zhao, S. Zhang and G. F. Pedersen, "SIW Multibeam Antenna Array at 30 GHz for 5G Mobile Devices," *IEEE Access*, vol. 7, pp. 73157-73164, 2019.

[9] F. Xu and K. Wu, "Guided-wave and leakage characteristics of substrate integrated waveguide", *IEEE Trans. Microw. Theory Techn.*, vol 53, no. 1, pp. 66-73, Jan. 2005.

[10] K. Wu, Y. J. Cheng, T. Djerafi and W. Hong, "Substrate-Integrated Millimeter-Wave and Terahertz Antenna Technology," *Proc. IEEE*, vol. 100, no. 7, pp. 2219-2232, July 2012.

[11] Y. Li and K. Luk, "Low-Cost High-Gain and Broadband Substrate-Integrated-Waveguide-Fed Patch Antenna Array for 60-GHz Band," *IEEE Trans. Antennas Propag.*, vol. 62, no. 11, pp. 5531-5538, Nov. 2014.

[12] W. Li, X. H. Tang and Y. Yang, "A Ka-Band Circularly Polarized Substrate Integrated Cavity-Backed Antenna Array," *IEEE Antennas Wireless Propag. Lett.*, vol. 18, no. 9, pp. 1882-1886, Sept. 2019.

[13] Y. Cai, Y. Zhang, Z. Qian and J. Liu, "A 16-element corporate-feed multilayer SIW cavity-backed slot antenna array," *IET Microw.Antennas Propag.*, vol. 11, no. 12, pp. 1796-1802, 22 9 2017.

[14] T. Y. Yang, W. Hong and Y. Zhang, "Wideband Millimeter-Wave Substrate Integrated Waveguide Cavity-Backed Rectangular Patch Antenna," *IEEE Antennas Wireless Propag. Lett.*, vol. 13, pp. 205-208, 2014.

[15] Q. Wu, J. Hirokawa, J. Yin, C. Yu, H. Wang and W. Hong, "Millimeter-Wave Multibeam Endfire Dual-Circularly Polarized Antenna Array for 5G Wireless Applications," *IEEE Trans. Antennas Propag.*, vol. 66, no. 9, pp. 4930-4935, Sept. 2018.

[16] Q. Wu, J. Hirokawa, J. Yin, C. Yu, H. Wang and W. Hong, "Z. Hao, Q. Yuan, B. Li and G. Q. Luo, "Wideband W -Band Substrate-Integrated Waveguide Magnetoelectric (ME) Dipole Array Antenna," *IEEE Trans. Antennas Propag.*, vol. 66, no. 6, pp. 3195-3200, June 2018.

[17] J. Liu, D. R. Jackson and Y. Long, "Substrate Integrated Waveguide (SIW) Leaky-Wave Antenna With Transverse Slots," *IEEE Trans. Antennas Propag.*, vol. 60, no. 1, pp. 20-29, Jan. 2012.

[18] D. K. Karmokar, S. Chen, D. Thalakotuna, P. Qin, T. S. Bird and Y. J. Guo, "Continuous Backward-to-Forward Scanning 1-D Slot-Array Leaky-Wave Antenna With Improved Gain," *IEEE Antennas Wireless Propag. Lett.*, vol. 19, no. 1, pp. 89-93, Jan. 2020.

[19] D. Zheng, Y. Lyu and K. Wu, "Transversely Slotted SIW Leaky-Wave Antenna Featuring Rapid Beam-Scanning for Millimeter-Wave Applications," *IEEE Trans. Antennas Propag.*, vol. 68, no. 6, pp. 4172-4185, June 2020.

[20] L. Wang, J. L. Gomez-Tornero and O. Quevedo-Teruel, "Substrate Integrated Waveguide Leaky-Wave Antenna With Wide Bandwidth via Prism Coupling," *IEEE Trans. Microw. Theory Techn.*, vol. 66, no. 6, pp. 3110-3118, June 2018.

[21] R. Hong, J. Shi, D. Guan, X. Huang, W. Cao and Z. Qian, "Air-Filled Substrate Integrated Waveguide Leaky-Wave Antenna with Wideband and Fixed-Beam Characteristics," *IEEE Trans. Antennas Propag.*, 2020.

[22] Y. Liu, H. Yang, Z. Jin, F. Zhao and J. Zhu, "Compact Rotman lens-fed slot array antenna with low sidelobes," *IET Microw.Antennas Propag.*, vol. 12, no. 5, pp. 656-661, 2018.

[23] J. Lian, Y. Ban, Z. Chen, B. Fu and C. Xiao, "SIW Folded Cassegrain Lens for Millimeter-Wave Multibeam Application," *IEEE Antennas Wireless Propag. Lett.*, vol. 17, no. 4, pp. 583-586, April 2018.

[24] A. B. Numan, J. Frigon and J. Laurin, "Printed W -Band Multibeam Antenna With Luneburg Lens-Based Beamforming Network," *IEEE Trans. Antennas Propag.*, vol. 66, no. 10, pp. 5614-5619, Oct. 2018.

[25] Y. J. Cheng, W. Hong and K. Wu, "Millimeter-Wave Substrate Integrated Waveguide Multibeam Antenna Based on the Parabolic Reflector Principle," *IEEE Trans. Antennas Propag.*, vol. 56, no. 9, pp. 3055-3058, Sept. 2008.

[26] Y. Cao, Y. Cai, L. Wang, Z. Qian and L. Zhu, "A Review of Substrate Integrated Waveguide End-Fire Antennas," *IEEE Access*, vol. 6, pp. 66243-66253, 2018.

[27] W. Stutzman and G. Thiele. *Antenna Theory and Design*, 3rd ed. Hoboken,NJ, USA: Wiley, 2013.

[28] L. Wang, X. Yin, S. Li, H. Zhao, L. Liu and M. Zhang, "Phase Corrected Substrate Integrated Waveguide H-Plane Horn Antenna With Embedded Metal-Via Arrays," *IEEE Trans. Antennas Propag.*, vol. 62, no. 4, pp. 1854-1861, April 2014.

[29] L. Wang, X. Yin and H. Zhao, "A Planar Feeding Technology Using Phase-and-Amplitude-Corrected SIW Horn and Its Application," *IEEE Antennas Wireless Propag. Lett.*, vol. 14, pp. 147-150, 2015.

[30] L. Wang, Esquius-Morote H. Qi, X. Yin, and J. R. Mosig. "Phase Corrected H-Plane Horn Antenna Gap SIW Technology", *IEEE Trans. Antennas Propag.*, vol. 65, no. 1, Jan. 2017

[31] N. Bayat-Makou and A. A. Kishk, "Substrate Integrated Horn Antenna With Uniform Aperture Distribution," *IEEE Trans. Antennas Propag.*, vol. 65, no. 2, pp. 514-520, Feb. 2017.

[32] H. Wang, Da-Gang Fang, B. Zhang, and Wen-Quan Che, "Dielectric Loaded Substrate Integrated Waveguide (SIW) H-Plane Horn Antennas", *IEEE Trans. Antennas Propag.*, vol. 58, no. 3, March 2010.

[33] L. Gong, Y. Fu, K. Y. Chan, J. A. Nanzer and R. Ramer, "An SIW Horn Antenna Fed by a Coupled Mode Emulating Pyramidal Horn Antennas," *IEEE Trans. Antennas Propag.*, vol. 68, no. 1, pp. 33-42, Jan. 2020.

[34] M. Esmaeili and J. Bornemann, "Coaxial-fed dual-layer SIW horn antenna with improved E-plane radiation pattern," in *47th European Microwave Conference (EuMC)*, Nuremberg, 2017, pp. 66-69.

[35] K. Wu, D. Deslandes, and Y. Cassivi, "The substrate integrated circuits - A new concept for high-frequency electronics and optoelectronics," in *Proc. 6th Int. Conf. Telecommun. Modern Satellite, Cable and Broadcasting*, Oct. 1–3, 2003, vol. 1, pp. P-III–P-X.

[36] A. Darvazehban, O. Manoochehri, M. A. Salari, P. Dehkhoda and A. Tavakoli, "Ultra-Wideband Scanning Antenna Array With Rotman Lens," *IEEE Trans. Microw. Theory Tech.*, vol. 65, no. 9, pp. 3435-3442, Sept. 2017.

[37] A. Tribak, J. Zbitou, A. Mediavilla Sanchez, and N. Amar Touhami, "Ultra-Broadband High Efficiency Mode Converter," *Prog. Electromagn. Res. C*, vol. 36, pp. 145-158, 2013.
[38] L. Wang, M. Garcia-Vigueras, M. Alvarez-Folgueiras, and J. R. Mosig, "Wideband H-plane dielectric horn antenna," *IET Microw.Antennas Propag.*, vol. 11, lss. 12, pp. 1695-1701, 2017.
[39] C. A. Balanis, *Antenna Theory: Analysis and Design*, 3rd ed. Hoboken, NJ, USA: Wiley, 2005.

CLEOFÁS SEGURA-GÓMEZ was born in Almería, Andalusia, Spain in 1997. He received the B.S. degree in Telecommunication Technologies Engineering from the University of Granada in 2019.

Since 2019 he has been studying for a M.S degree in Telecommunications Engineering at the University of Granada. Also, he has been researching in SIW antennas within SWAT research group in Granada.

ÁNGEL PALOMARES-CABALLERO was born in Jaen, Spain, in 1994. He received the B.Sc. and M.Sc.degrees in telecommunication engineering from the University of Granada (UGR), Granada, Spain, in 2016 and 2018, respectively. Since 2017, he has been with the Department of Signal Theory, Telematics and Communications, University of Granada, where he is currently a Ph.D.student with a national Predoctoral Fellowship. His current research interests include millimeter-wave antennas and phase shifters, gap waveguide, and structures with higher symmetries.

ANTONIO ALEX-AMOR received the B.Sc. degree in telecommunication engineering from Universidad de Granada, in 2016, and the M.Sc. degree in telecommunication engineering from Universidad Politécnica de Madrid (UPM), in 2018, where he is currently pursuing the Ph.D. degree. Since 2016, he has been with the Radiation Group, Signal, Systems and Radiocommunications Department, UPM. From 2018-2019, he joined the Department of Language and Computer Science, Universidad de Málaga. In 2020, he joined the Departamento de Teoría de la Señal, Telemática y Telecomunicaciones, Universidad de Granada. He received the Best Electromagnetics Paper Award at the 14th European Conference on Antennas and Propagation (EuCAP 2020). His current research interests include the use of liquid crystal as tunable dielectric, metamaterials, structures with higher symmetries and radiofrequency energy harvesting systems.

JUAN VALENZUELA-VALDÉS was born in Marbella, Spain. He received the degree in telecommunications engineering from the Universidad de Malaga, Spain, in 2003, and the Ph.D. degree from the Universidad Politécnica de Cartagena, Spain, in 2008, where he joined the Department of Information Technologies and Communications, in 2004. In 2007, he joined EMITE Ing. as the Head of research. In 2011, he joined the Universidad de Extremadura, and in 2015, he joined the Universidad de Granada, where he is currently an Associate Professor. His current research interests include wireless communications and efficiency in wireless sensor networks. He has also received several prizes, including a National Prize to the Best Ph.D. in Mobile Communications by Vodafone and the i-Patentes Award by the Spanish Autonomous Region of Murcia for innovation and technology transfer excellence. He is the Co-Founder of Emite Ing, a spin-off company. He also holds several national and international patents. His publication record comprised of more than 80 publications, including 40 JCR indexed articles, more than 30 contributions in international conferences, and seven book chapters

PABLO PADILLA was born in Jaén, Spain, in 1982. He received the Telecommunication Engineering degree and the Ph.D. degree from the Radiation Group (Signal, Systems and Radiocommunications Department) of the Technical University of Madrid (UPM), Spain, in 2005 and 2009, respectively. In 2007, he was with the Laboratory of Electromagnetics and Acoustics, École Polytechnique Fédérale de Lausanne, Switzerland, as an invited Ph.D. Student. In 2009, he carried out a Postdoctoral stay at the Helsinki University of Technology (AALTO-TKK). In 2009, he became Assistant Professor at the Signal Theory, Telematics and Communications Department of the University of Granada, where he is currently Associate Professor, since 2012. In 2017, he was an invited Visiting Professor at the Royal Institute of Technology of Stockholm. He has authored more than 65 high-impact journal contributions and more than 60 contributions to international symposia. His research interests include a variety of topics related mainly to electromagnetism and communication issues (radiofrequency devices, antennas and propagation).